Scientific Reports

https://doi.org/10.1038/s41598-026-42861-w

Article in Press

Gamma-aminobutyric acid transaminase mediates tumor suppression in renal cell carcinoma through the cGAS-STING–interferon-β axis

Received: 12 December 2025

Accepted: 27 February 2026

Published online: 11 March 2026

Cite this article as: Feng Y., Cao S., Cai T. *et al.* Gamma-aminobutyric acid transaminase mediates tumor suppression in renal cell carcinoma through the cGAS-STING–interferon-β axis. *Sci Rep* (2026). https://doi.org/10.1038/s41598-026-42861-w

Yi Feng, Senming Cao, Tianwei Cai, Yin Lu, Bin Jiang, Zexuan Lv, Jinlu Tang, Fan Gao, Xupeng Zhao, Chunyu Liu, Qi Wang, Ji Feng, Zheng Wang, Qing Ai, Qiang Cheng, Wenmei Fan & Hongzhao Li

Gamma-aminobutyric acid transaminase mediates tumor suppression in renal cell carcinoma through the cGAS-STING–interferon-β axis

Yi Feng[1,2,3#], Senming Cao[1,2,4#], Tianwei Cai[1,2,3#], Yin Lu[1,4], Bin Jiang[1,3], Zexuan Lv[1,4], Jinlu Tang[1,3], Fan Gao[1,2,4], Xupeng Zhao[1], Chunyu Liu[1,2,3], Qi Wang[1,2,3], Ji Feng[1,2,3], Zheng Wang[1,2,3], Qing Ai[1], Qiang Cheng[1,2*], Wenmei Fan[1,2*], Hongzhao Li[1*].

[1]Department of Urology, The Third Medical Center of PLA General Hospital, Beijing, China.

[2]Department of Urology Laboratory, Chinese PLA General Hospital, Beijing, China.

[3]Medical School of PLA, Beijing, China.

[4]Medical School of NanKai University, TianJing, China.

*** Corresponding author:**

Hongzhao Li

urolancet@126.com

Wenmei Fan

fan_wenmei@163.com

Qiang Cheng

cxqyisheng@126.com

[#]These authors have contributed equally to this work.

Abstract

Clear cell renal cell carcinoma (ccRCC) is resistant to conventional radiotherapy and chemotherapy, creating an urgent need for novel therapeutic strategies. Although GABA transaminase (ABAT) is involved in metabolic reprogramming as reported, its precise function and molecular mechanisms in ccRCC remain unclear. Here, we demonstrate that ABAT overexpression suppresses tumor growth both in vitro and in vivo. Mechanistically, ABAT mediates the cGAS–STING signaling pathway, and interacts with protein arginine methyltransferase 5 (PRMT5), thereby enhances interferon signaling. Besides, ABAT was found to reduce the infiltration of regulatory

T cells within the tumor microenvironment. Collectively, these results suggest that ABAT represents a potential therapeutic target in clear cell renal cell carcinoma.

Key Words

Gamma-aminobutyric acid transaminase, ccRCC,cGAS-STING, IFN-β , PRMT5.

Introduction

It is estimated that over 400,000 new cases of kidney cancer are diagnosed and more than 175,000 related deaths occur worldwide each year [1] . The most common type is renal cell carcinoma (RCC), which accounts for 80% to 90% of all kidney cancer cases. RCC comprises a heterogeneous group of cancers originating from renal tubular epithelial cells [2] . Among its various pathological subtypes, clear cell RCC (ccRCC) is the most prevalent, representing approximately 65% of RCC and responsible for the majority of RCC-related deaths [3, 4] .

Localized ccRCC remains primarily treated by surgical resection[5]; nevertheless, 20–30% of patients develop metastatic recurrence after surgery[6]. Moreover, 30–50% of patients present with metastatic disease at initial diagnosis, which is generally associated with a poorer prognosis [7] .ccRCC is not sensitive to radiotherapy or chemotherapy, and current treatments are mainly based on targeted therapy and immunotherapy. Therefore, the discovery of new targets for ccRCC still has significant clinical implications.

Accumulating evidence suggests that gamma-aminobutyric acid (GABA) is involved in tumor progression. Although GABA functions as a neurotransmitter in the central nervous system and scarcely crosses the blood-brain barrier, growing evidence indicates its accumulation in non-neuronal tumors—such as lung cancer, colorectal cancer, and melanoma—where it promotes tumorigenesis [8-11] . In vivo, GABA metabolism and catabolism are associated with the enzyme gamma-aminobutyric acid transaminase (ABAT) [12] . Recent studies have shown that ABAT expression is decreased in ccRCC and that it suppresses the oncogenic capacity of ccRCC cells [13] . Nevertheless, the intrinsic function and underlying mechanisms of ABAT in ccRCC remain unexplored.

Here, we report that ABAT directly exerts tumor-killing effects by enhancing interferon signaling mediated via the cGAS–STING pathway.

Results

ABAT expression is significantly downregulated in renal cell carcinoma.

GABA in the human body is maintained in a dynamic equilibrium, primarily synthesized by glutamate decarboxylase 1 (GAD1) and metabolized by ABAT [12] . To clarify the expression levels of ABAT and GAD1 in kidney cancer patients, we queried The Cancer Genome Atlas Program (TCGA) database. The results indicate that both ABAT and GAD1 are significantly downregulated in renal carcinoma. However, the decrease in ABAT is associated with a poorer prognosis, whereas the expression level of GAD1 shows no significant correlation with patient outcomes （figure1，A and B) . Subsequently, we collected five paired clinical samples from our institution. The immunohistochemical and RT-qPCR results(figure1,B-D) were consistent with the findings from the public databases. Therefore, we decided to further investigate the role of ABAT.

Overexpression of ABAT significantly suppressed tumor growth.

To investigate the function of ABAT in tumors, we overexpressed the *ABAT* gene in two human ccRCC cell lines (OSRC2 and A498)(figure1,E and figure2A). Both EdU staining assays and CCK-8 assays demonstrated that ABAT overexpression significantly inhibited the proliferation of ccRCC cells.The wound healing and Transwell assays also indicated the tumor-suppressive function of ABAT(figure2B-E). Moreover, knocking down the *ABAT gene* in the ABAT-overpressing cells markedly attenuated this suppressive effect on cell proliferation(figure2C).To examine the impact of ABAT on tumor growth in vivo, OSRC2 cells overexpressing ABAT were subcutaneously injected into the flanks of nude mice. The results showed that ABAT overexpression significantly reduced both the growth rate and final size of the tumors(figure2F).

To determine whether the function of ABAT in ccRCC depends on its Enzyme Function, exogenous GABA was added to the culture, followed by EdU staining and measurement of GABA levels in the cell supernatant using an ELISA kit(figure2G). The results indicated that GABA levels in the supernatant were significantly decreased in ABAT-overexpressing cells, yet this did not interfere with tumor cell growth(figure2H). This series of experiments suggests that ABAT inhibits ccRCC cell growth, independent of its enzymatic role in GABA catabolism.

Overexpression of ABAT triggers cGAS-STING-induced type I interferon (IFN-I) signaling.

To further decipher the mechanism by which ABAT attenuates tumor growth, we performed RNA-seq analysis on OSRC2 cells overexpressing ABAT. Analysis of differentially expressed genes revealed that many of the top-ranked genes were interferon-stimulated genes (e.g., MX1, MX2, ISG15, ISG20)(figure3A and B). Reactome pathway enrichment analysis indicated that these differentially expressed genes were primarily enriched in the IFN signaling pathway and the IFN alpha/beta signaling pathway(figure3C-F). We then validated the RNA-seq data by qRT-PCR, confirming that ABAT overexpression significantly elevated the transcript levels of these ISGs and IFN-β(figure3G). Subsequently, an ELISA kit was used to detect IFNβ levels in the cell culture supernatant, which showed a significant increase in ABAT-overexpressing ccRCC cell lines. Western blot analysis further supported this result(figure3H-I).

According to published literature, IFN-β secretion is triggered by the activation of the upstream transcription factor interferon regulatory factor 3 (IRF3). Several innate sensing pathways are involved in this regulatory process, such as the dsDNA sensor cGAS-STING, the dsRNA sensor RIG-I/MDA5-MAVS, and the LPS sensor Toll-like receptors [14, 15]. To identify which sensor plays a critical role in ABAT-promoted IFN-β secretion, we treated ABAT-overexpressing cells with inhibitors targeting different sensor pathways. The results showed that adding H151, an inhibitor of the cGAS-STING pathway [16], but not RIG012, an inhibitor of the

RIG-I/MDA5-MAVS pathway [17] , significantly reduced the IFN-β levels induced by ABAT overexpression(figure3,I-K and figure4,A and B). In vivo experiments also demonstrated that treatment with H151 partially rescued the tumor-suppressive effect caused by ABAT overexpression. Therefore, we conclude that the cGAS-STING pathway responds to changes in ABAT levels, thereby activating IFN-β(figure3L).

Overexpression of ABAT affects mitochondrial homeostasis and interacts with PRMT5.

Next, we sought to investigate the mechanism by which ABAT regulates the cGAS-STING pathway. We transfected FLAG-ABAT plasmids into OSRC2 and A498 cells and performed co-immunoprecipitation (co-IP) followed by mass spectrometry analysis of the associated proteins(figure4C). Among the identified proteins, protein arginine methyltransferase 5 (PRMT5) [18, 19] showed high confidence scores in both cell lines(figure4D). Western blot analysis confirmed the interaction between ABAT and PRMT5(figure4E). The immunofluorescence results further corroborate the co-localization between the two(figure4J). Subsequently, we knocked down the *PRMT5* gene in OSRC2 cells and observed that PRMT5 knockdown significantly increased the level of phosphorylated STING and IFN-β (figure4F-H).

Notably, ABAT is a mitochondrial matrix protein, whereas PRMT5 is predominantly reported to localize in the cytoplasm and nucleus [20-23] . We hypothesized that ABAT overexpression might induce mitochondrial stress, leading to the release of ABAT into the cytoplasm due to mitochondrial damage. To examine mitochondrial status, we utilized the dsDNA probe PicoGreen and performed RT-qPCR to detect cytoplasmic mitochondrial DNA (mtDNA) [24] （figure4I and figure5A). The results showed that cells overexpressing ABAT released more dsDNA into the cytoplasm. Furthermore, using the JC-1 probe [25] , we observed a decrease in mitochondrial membrane potential in ABAT-overexpressing cells(figure5B-E). Cryo-electron microscopy also revealed abnormal mitochondrial morphology in these

cells(figure5). Collectively, these findings indicate that ABAT overexpression induces mitochondrial damage.

ABAT Reduces Treg Cell Infiltration in the Immune Microenvironment

Next, we sought to clarify how ABAT functions within an immune-competent context. We performed subcutaneous tumor implantation experiments using BALB/c mice. Consistent with previous findings, tumor formation by Renca cells overexpressing ABAT was significantly suppressed in immunocompetent mice(figure5G). To explore the underlying mechanism, we used flow cytometry to analyze immune cell populations in control and ABAT-overexpressing ccRCC tumors; the gating strategy for murine tumor-infiltrating immune cells is provided in the Supplementary Methods(Supplemental Figure1A). We found that ABAT overexpression markedly reduced the infiltration of regulatory T cells (Tregs). Although the number of $CD8^+$ T cells did not show a significant change, the ratio of Tregs to $CD8^+$ T cells was considerably decreased(figure5H). These results suggest that ABAT may alleviate the immunosuppressive state in the tumor microenvironment by inhibiting the recruitment of Tregs. However, the precise mechanism involved requires further investigation.

Discussion

Advanced ccRCC is associated with a poor prognosis, and while TKIs constitute a mainstay of clinical therapy, a subset of patients fails to benefit from these treatments【26】. The discovery of novel therapeutic targets remains imperative, especially as the demand for precision medicine in kidney cancer patients continues to rise. Our study demonstrates that ABAT suppresses ccRCC cells by activating innate immunity. Given that ABAT expression is commonly downregulated in ccRCC patients, lower ABAT levels appear to promote cancer cell survival. Our findings identify ABAT as a potential therapeutic target for ccRCC. However, the mechanisms by which ccRCC drives the reduction of ABAT levels remain to be elucidated.

PRMT5 is currently recognized as an oncogene in multiple cancer types [27-31], and its inhibitors have already entered clinical trials [32-34]. PRMT5 and its metabolites have also been reported to be involved in renal tumor [35]. Our experiments indicate an interaction between ABAT and PRMT5, which further suggests the potential utility of PRMT5 inhibitors in renal cancer. Regarding the mechanism underlying their interaction, we propose two possible explanations: mitochondrial damage induced by ABAT overexpression, or the recruitment of PRMT5 to the mitochondrial outer membrane by ABAT. There is accumulating evidence that PRMT5 plays a crucial role in mitochondrial function [36, 37]. If we can elucidate the mechanism of interaction between PRMT5 and mitochondria, it would represent a significant innovative contribution.

ccRCC is also a highly immunogenic tumor, characterized by a substantial presence of immune cells exhibiting a suppressive phenotype [38, 39]. Increasing evidence suggests that combination therapy using TKIs and immune checkpoint inhibitors holds considerable promise [40-42]. Our study demonstrates that ABAT alleviates the immunosuppressive state in renal cell carcinoma by reducing Treg infiltration.This finding highlights the potential value of ABAT in the context of immunotherapy.

However, our study still has many limitations. For instance, knocking down *ABAT* resulted in cell growth, which led us to use only overexpression models rather than knockdown approaches. Additionally, PRMT5 has been reported to suppress the activation of STING [43-45]. Given that ABAT overexpression impairs mitochondrial integrity and thereby establishes a permissive environment for cGAS–STING activation, whether PRMT5 contributes to this process remains to be elucidated. Previous studies have reported that ABAT drives sunitinib resistance in renal cell carcinoma through metabolic reprogramming [46]. As a metabolic enzyme, whether its substrate GABA plays a role in our experimental system remains unclear, as we were unable to successfully construct enzymatic active-site mutants. Furthermore, the

potential role of GABA in an intact immune context has yet to be examined. These questions warrant further in-depth exploration in subsequent studies.

In summary, our study reveals that ABAT mediates the cGAS – STING signaling pathway to promote IFN-β release, thereby exerting cytotoxic effects on ccRCC cells. This finding may offer a new therapeutic target for metastatic and advanced renal cell carcinoma.

METHODS

Human Samples and Animal Models

Human renal cancer samples from both male and female patients were analyzed. All mouse studies included both male and female animals; sex was not considered as a biological variable in this study.

Cell Lines and Clinical Specimens

The ccRCC cell lines OSRC2 and A498, as well as the mouse renal carcinoma cell line Renca, were purchased from Bionovogene Co., Ltd. OSRC2 and Renca were cultured in RPMI-1640 medium (Procell), and A498 was maintained in MEM medium (Procell). All media were supplemented with 10% FBS (Procell) and 1% penicillin–streptomycin (Procell), except for Renca which was cultured with 20% FBS. Cells were incubated at 37°C under 5% CO_2. All cell lines were routinely confirmed to be free of mycoplasma contamination. Surgically resected human ccRCC tissues and associated clinical information were obtained from the Department of Urology, Chinese PLA General Hospital. Histology and pathological subtypes of all tissues were independently confirmed by three experienced pathologists.

Plasmid Construction and Transfection

The coding sequence (CDS) of the human ABAT gene was synthesized by Biomed and cloned into the pCMV-Flag vector. The mouse ABAT CDS was also synthesized by Biomed and cloned into the pCMV vector. Lentiviral vectors were co-transfected with PAX2 and VSVG packaging plasmids into HEK293T cells. After 48–72 h, supernatants were collected and concentrated overnight at 4°C using a lentivirus concentration reagent (GenStar). To generate stable cell lines, cells were infected with lentivirus for 24 h followed by puromycin selection for one week.

Cell Viability Assay

For proliferation assays, OSRC2 and A498 cells were seeded in 96-well plates at 2,000 cells per well in 100 µL complete medium. Viability was assessed every 24 h by adding CCK-8 reagent to each well, incubating at 37°C for 2 h, and measuring absorbance with a microplate reader.

EdU Assay

Cells were seeded at 5×10^4 per well in 96-well plates. EdU incorporation was detected using the BeyoClick™ EdU Cell Proliferation Kit (Beyotime, C0078S). In brief, cells were incubated with EdU working solution for 2 h at 37°C, fixed with 4% paraformaldehyde, permeabilized with 0.1% Triton X-100, and reacted with Click reaction solution. Nuclei were counterstained with Hoechst. Fluorescent images were captured under a microscope, and five random fields per well were quantified.

Quantitative Real-Time PCR (qRT-PCR)

Total RNA was extracted using the FastPure Cell/Tissue Total RNA Isolation Kit V2 (Vazyme). cDNA was synthesized with HiScript III RT SuperMix (Vazyme). qPCR was performed using ChamQ Universal SYBR qPCR Master Mix (Vazyme) on a CFX96 Real-Time PCR System (Bio-Rad). Gene expression fold-changes were calculated after normalization to GAPDH. Primer sequences are listed in Supplementary Table X.

Invasion Assay

For invasion assays, 2×10^4 cells in 200 μL serum-free medium were seeded into the upper chamber of a 24-well Transwell insert pre-coated with 5% Matrigel. The lower chamber contained 600 μL medium with 10% FBS. After 24 h, invaded cells were fixed with 4% paraformaldehyde, stained with 0.1% crystal violet, and counted in three random fields.

Western Blotting

Cells were lysed on ice for 30 min using RIPA buffer containing protease inhibitors and PMSF. Protein concentration was determined with a BCA Protein Assay Kit (Solarbio). Samples were denatured in 5× loading buffer at 95°C for 10 min, separated by SDS-PAGE, and transferred to PVDF membranes. Membranes were blocked with 5% non-fat milk, incubated overnight at 4°C with primary antibodies against GAPDH (Proteintech, 60004-1-Ig), ABAT (Zenbio, R24385), STING pathway proteins (Human-Reactive STING Pathway Antibody Sampler Kit), and IFN-β (Proteintech, 27506-1-AP). After washing, membranes were incubated with HRP-conjugated anti-rabbit (Proteintech, SA00001-2) or anti-mouse (Proteintech, SA00001-1) secondary antibodies for 1 h at room temperature. Protein bands were visualized using an ECL substrate on a QuickChemi 5200 imaging system.

Immunohistochemistry (IHC)

Paraffin-embedded tissue sections were stained for ABAT and GAD1 expression. Sections were incubated overnight at 4°C with primary antibodies against ABAT (Zenbio, R24385) and GAD1 (Proteintech, 10408-1-AP), followed by enzyme-conjugated secondary antibodies. After washing, color development was performed with DAB substrate. Staining intensity was evaluated based on the percentage of positive cells.

Animal Studies

All animal experiments were approved by the Institutional Animal Care and Use Committee. BALB/c and nude mice (6–8 weeks old) were purchased from Beijing Vital River Laboratory Animal Technology Co., Ltd. Mice were housed under a 12-h light/dark cycle with free access to food and water in a specific pathogen-free facility.**Avertin (Tribromoethanol) Solution Preparation**: An anesthetic stock solution (1.25% w/v) was prepared by dissolving 2.5 g of 2,2,2-tribromoethanol in 5 mL of tertiary amyl alcohol (2-methyl-2-butanol). The final volume was adjusted to 200 mL with sterile ultrapure water. The solution was protected from light and filtered through a 0.22 μm sterile filter prior to use.**Mouse Anesthesia**: Mice were anesthetized via intraperitoneal (i.p.) injection of the freshly prepared 1.25% tribromoethanol solution at a standard dosage of 20 μL per gram of body weightThe body weight of the mice was 200 ± 20 g..**Euthanasia**: To minimize distress and ensure a humane endpoint, anesthetized mice were euthanized by cervical dislocation.Animal experiments have been subjected to ethical review, approval number: ZYZC202511006S.

Subcutaneous Tumorigenesis

Renca (2×10^6 cells/mouse) or OSRC2 (5×10^6 cells/mouse) cells were injected subcutaneously into the right flank of BALB/c or nude mice. Tumor size was measured every two days using calipers once tumors became palpable, and volume was calculated as (length × width²)/2. For rescue experiments, starting from day 14, mice were intraperitoneally injected every two days with 7.5 μM H151 (MCE, HY-112693) or PBS as control.

ELISA

Cell culture supernatants were collected from 6-well plates. Levels of human IFN-β were measured using a commercial ELISA kit (Elabscience) according to the manufacturer's instructions. Cytokine concentrations were calculated based on OD values at 450 nm.

RNA-seq and GSEA

Total RNA was isolated using the FastPure Cell/Tissue Total RNA Isolation Kit V2 (Vazyme). RNA sequencing and library preparation were performed by Majorbio Bio-Pharm Technology Co., Ltd. on an Illumina platform. Differentially expressed genes were defined as those with $|\log_2 FC| > 1.5$ and adjusted $p \leq 0.05$. Gene set enrichment analysis (GSEA) was conducted using the Molecular Signatures Database (MSigDB) to evaluate IFN-I-related signatures.

Cytosolic mtDNA Detection

OSRC2 or A498 cells were seeded in 6-well plates. Cells were treated on ice with NP-40 buffer for 15 min. Supernatants were collected and centrifuged at 18,630 ×g for 15 min at 4°C. DNA was extracted from the supernatant using the Beyotime

Genomic DNA Extraction Kit. mtDNA levels were quantified by RT-qPCR or conventional PCR.

Mitochondrial Membrane Potential (ΔΨm) Measurement

ΔΨm was assessed using the fluorescent dye JC-1. Cells were incubated with 2–5 μM JC-1 staining solution at 37°C for 20–30 min in the dark, washed with pre-warmed PBS, and analyzed immediately. Fluorescence was detected using a fluorescence microscope or microplate reader. JC-1 forms red-fluorescent aggregates (Ex/Em 525/590 nm) at high ΔΨm and green-fluorescent monomers (Ex/Em 490/530 nm) at low ΔΨm. The ratio of red to green fluorescence intensity was used to represent ΔΨm; a decrease in the ratio indicates mitochondrial depolarization.

Flow Cytometric Analysis of Tumor-Infiltrating Immune Cells

Tumor-bearing mice were euthanized, and tumors were excised, weighed, and mechanically dissociated. Tissues were digested with DNase I and collagenase IV (Sigma-Aldrich) at 37°C for 60 min. Single-cell suspensions were obtained by filtering through a 70-μm strainer (BIOFIL). After washing with RPMI-1640, red blood cells were lysed (Beyotime). Cells were stained in the dark for 30 min with the following antibodies: BV510 anti-mouse CD45 (BioLegend, 103137), BV605 anti-mouse CD3 (BioLegend, 100237), Alexa Fluor 488 anti-mouse CD4 (BioLegend, 100423), APC/Fire 750 anti-mouse CD8a (BioLegend, 100766), and APC anti-mouse NK1.1 (BioLegend, 108710). Stained cells were analyzed by flow cytometry (BD Biosciences), and data were processed using FlowJo software.

Statistical Analysis

Data are presented as mean ± SD. Overall survival was calculated using the Kaplan–Meier method with the log-rank test. Differences between groups were assessed by two-tailed Student's t-test, one-way ANOVA, or two-way ANOVA, as appropriate. Statistical analyses were performed using GraphPad Prism software. A p-value < 0.05 was considered statistically significant.

Study approval.

All Kidney cancer tissue samples used in this study were obtained from patients with their informed consent, and the use of these samples was approved by the IRB of the Chinese PLA General Hospital. All animal experiments were performed in accordance with institutional regulations and approval by the Institutional Animal Care and Use Committee of the Chinese PLA General Hospital.

Data availability.

The datasets generated and analysed during the current study are available in the NCBI Sequence Read Archive . (SRR36638439, SRR36638436, SRR36638441, SRR36638438, SRR36638440, SRR36638437)

Author contributions

Yi Feng was responsible for conceptualization, data curation, formal analysis, investigation, methodology, and writing of the original draft. Senming Cao was responsible for investigation and methodology. Tianwei Cai was responsible for formal analysis, validation, and methodology. Yin Lu was responsible for formal analysis and investigation. Bin Jiang was responsible for formal analysis and investigation. Zexuan Lv was responsible for formal analysis and investigation. Jinlu Tang was responsible for investigation. Chunyu Liu was responsible for investigation. Qi Wang was responsible for formal analysis. Ji Feng was responsible for investigation. Zheng Wang was responsible for resources. Qi Ai was responsible for resources. Xupeng Zhao was responsible for resources. KL was responsible for conceptualization and data curation. Qiang Cheng was responsible for conceptualization, data curation, and funding acquisition. Wenmei Fan was responsible for conceptualization, resources, supervision, and funding acquisition. Hongzhao Li was responsible for conceptualization, resources, data curation, formal analysis, supervision, funding acquisition, and writing of the original draft.

Funding Statement

This study received financial support from the Ministry of Science and Technology of the People's Republic of China.（Hongzhao Li，2022YFC3602901）

Competing interests

The authors declare no competing interests.

Ethics approval

Renal tissue samples were acquired from the Kidney Biobank of the Department of Urology at the Chinese PLA General Hospital during the period spanning January to December 2019. The study protocol involving human specimens received ethical approval from the Chinese PLA General Hospital Ethics Committee (Approval No. S2013-065-01).

Confirming

the study is reported in accordance with ARRIVE guidelines. All methods were carried out in accordance with relevant guidelines and regulations.

Reference

[1] Huang J, Leung DK, Chan EO, et al. A Global Trend Analysis of Kidney Cancer Incidence and Mortality and Their Associations with Smoking, Alcohol Consumption, and Metabolic Syndrome. [J]. Eur Urol Focus, 2022,8,200. http://dx.doi.org/10.1016/j.euf.2020.12.020.

[2] Lindgren D, Sjölund J and Axelson H. Tracing Renal Cell Carcinomas back to the Nephron. [J]. Trends Cancer, 2018,4,472. http://dx.doi.org/10.1016/j.trecan.2018.05.003.

[3] Jonasch E, Gao J and Rathmell WK. Renal cell carcinoma. [J]. Bmj, 2014,349,g4797. http://dx.doi.org/10.1136/bmj.g4797.

[4] Chen F, Zhang Y, Şenbabaoğlu Y, et al. Multilevel Genomics-Based Taxonomy of Renal Cell Carcinoma. [J]. Cell Rep, 2016,14,2476. http://dx.doi.org/10.1016/j.celrep.2016.02.024.

[5] Hsieh JJ, Purdue MP, Signoretti S, et al. Renal cell carcinoma. [J]. Nat Rev Dis Primers, 2017,3,17009. http://dx.doi.org/10.1038/nrdp.2017.9.

[6] He Y, Ma X, Chen K, et al. Perioperative Circulating Tumor DNA in Colorectal Liver Metastases: Concordance with Metastatic Tissue and Predictive Value for Tumor Burden and Prognosis. [J]. Cancer Manag Res, 2020,12,1621. http://dx.doi.org/10.2147/cmar.S240869.

[7] Siegel RL, Miller KD and Jemal A. Cancer statistics, 2015. [J]. CA Cancer J Clin, 2015,65,5. http://dx.doi.org/10.3322/caac.21254.

[8] Zhang B, Vogelzang A, Miyajima M, et al. B cell-derived GABA elicits IL-10(+) macrophages to limit anti-tumour immunity. [J]. Nature, 2021,599,471. http://dx.doi.org/10.1038/s41586-021-04082-1.

[9] Tagore M, Hergenreder E, Perlee SC, et al. GABA Regulates Electrical Activity and Tumor Initiation in Melanoma. [J]. Cancer Discov, 2023,13,2270. http://dx.doi.org/10.1158/2159-8290.Cd-23-0389.

[10] Xie M, Qin H, Liu L, et al. GABA regulates metabolic reprogramming to mediate the development of brain metastasis in non-small cell lung cancer. [J]. J Exp Clin Cancer Res, 2025,44,61. http://dx.doi.org/10.1186/s13046-025-03315-9.

[11] Huang D, Wang Y, Thompson JW, et al. Cancer-cell-derived GABA promotes β-catenin-mediated tumour growth and immunosuppression. [J]. Nat Cell Biol, 2022,24,230. http://dx.doi.org/10.1038/s41556-021-00820-9.

[12] Zhang Q, Zhu L, Li H, et al. Insights and progress on the biosynthesis, metabolism, and physiological functions of gamma-aminobutyric acid (GABA): a review. [J]. PeerJ, 2024,12,e18712. http://dx.doi.org/10.7717/peerj.18712.

[13] Lu J, Chen Z, Zhao H, et al. ABAT and ALDH6A1, regulated by transcription factor HNF4A, suppress tumorigenic capability in clear cell renal cell carcinoma. [J]. J Transl Med, 2020,18,101. http://dx.doi.org/10.1186/s12967-020-02268-1.

[14] Zhao B, Shu C, Gao X, et al. Structural basis for concerted recruitment and activation of IRF-3 by innate immune adaptor proteins. [J]. Proc Natl Acad Sci U S A, 2016,113,E3403. http://dx.doi.org/10.1073/pnas.1603269113.

[15] Zhuang Q, Dai Z, Xu X, et al. RNA Methyltransferase FTSJ3 Regulates the Type I Interferon Pathway to Promote Hepatocellular Carcinoma Immune Evasion. [J]. Cancer Res, 2024,84,405. http://dx.doi.org/10.1158/0008-5472.Can-23-2049.

[16] Haag SM, Gulen MF, Reymond L, et al. Targeting STING with covalent small-molecule inhibitors. [J]. Nature, 2018,559,269. http://dx.doi.org/10.1038/s41586-018-0287-8.

[17] Rawling DC, Jagdmann GE, Jr., Potapova O, et al. Small-Molecule Antagonists of the RIG-I Innate Immune Receptor. [J]. ACS Chem Biol, 2020,15,311. http://dx.doi.org/10.1021/acschembio.9b00810.

[18] Engstrom LD, Aranda R, Waters L, et al. MRTX1719 Is an MTA-Cooperative PRMT5 Inhibitor That Exhibits Synthetic Lethality in Preclinical Models and Patients with MTAP-Deleted Cancer. [J]. Cancer Discov, 2023,13,2412. http://dx.doi.org/10.1158/2159-8290.Cd-23-0669.

[19] Kalev P, Hyer ML, Gross S, et al. MAT2A Inhibition Blocks the Growth of MTAP-Deleted Cancer Cells by Reducing PRMT5-Dependent mRNA Splicing and Inducing DNA Damage. [J]. Cancer Cell, 2021,39,209. http://dx.doi.org/10.1016/j.ccell.2020.12.010.

[20] Lacroix M, El Messaoudi S, Rodier G, et al. The histone-binding protein COPR5 is required for nuclear functions of the protein arginine methyltransferase PRMT5. [J]. EMBO Rep, 2008,9,452. http://dx.doi.org/10.1038/embor.2008.45.

[21] Andreu-Pérez P, Esteve-Puig R, de Torre-Minguela C, et al. Protein arginine methyltransferase 5 regulates ERK1/2 signal transduction amplitude and cell fate through CRAF. [J]. Sci Signal, 2011,4,ra58. http://dx.doi.org/10.1126/scisignal.2001936.

[22] Guderian G, Peter C, Wiesner J, et al. RioK1, a new interactor of protein arginine methyltransferase 5 (PRMT5), competes with pICln for binding and modulates PRMT5 complex composition and substrate specificity. [J]. J Biol Chem, 2011,286,1976. http://dx.doi.org/10.1074/jbc.M110.148486.

[23] El-Hattab AW, Craigen WJ and Scaglia F. Mitochondrial DNA maintenance defects. [J]. Biochim Biophys Acta Mol Basis Dis, 2017,1863,1539. http://dx.doi.org/10.1016/j.bbadis.2017.02.017.

[24] Liu H, Zhen C, Xie J, et al. TFAM is an autophagy receptor that limits inflammation by binding to cytoplasmic mitochondrial DNA. [J]. Nat Cell Biol, 2024,26,878. http://dx.doi.org/10.1038/s41556-024-01419-6.

[25] Lyu Q, Yang Q, Hao J, et al. A small proportion of X-linked genes contribute to X chromosome upregulation in early embryos via BRD4-mediated transcriptional activation. [J]. Curr Biol, 2022,32,4397. http://dx.doi.org/10.1016/j.cub.2022.08.059.

[26] George DJ, Lee CH and Heng D. New approaches to first-line treatment of advanced renal cell carcinoma. [J]. Ther Adv Med Oncol, 2021,13,17588359211034708. http://dx.doi.org/10.1177/17588359211034708.

[27] Wang Z, Li R, Hou N, et al. PRMT5 reduces immunotherapy efficacy in triple-negative breast cancer by methylating KEAP1 and inhibiting ferroptosis. [J]. J Immunother Cancer, 2023,11,http://dx.doi.org/10.1136/jitc-2023-006890.

[28] Liu A, Yu C, Qiu C, et al. PRMT5 methylating SMAD4 activates TGF-β signaling and promotes colorectal cancer metastasis. [J]. Oncogene, 2023,42,1572. http://dx.doi.org/10.1038/s41388-023-02674-x.

[29] Jiang Y, Yuan Y, Chen M, et al. PRMT5 disruption drives antitumor immunity in cervical cancer by reprogramming T cell-mediated response and regulating PD-L1 expression. [J]. Theranostics, 2021,11,9162. http://dx.doi.org/10.7150/thno.59605.

[30] Yan W, Liu X, Qiu X, et al. PRMT5-mediated FUBP1 methylation accelerates prostate cancer progression. [J]. J Clin Invest, 2024,134,http://dx.doi.org/10.1172/jci175023.

[31] Frau M, Feo F and Pascale RM. Pleiotropic effects of methionine adenosyltransferases deregulation as determinants of liver cancer progression and prognosis. [J]. J Hepatol, 2013,59,830. http://dx.doi.org/10.1016/j.jhep.2013.04.031.

[32] Belmontes B, Slemmons KK, Su C, et al. AMG 193, a Clinical Stage MTA-Cooperative PRMT5 Inhibitor, Drives Antitumor Activity Preclinically and in Patients with MTAP-Deleted Cancers. [J]. Cancer Discov, 2025,15,139. http://dx.doi.org/10.1158/2159-8290.Cd-24-0887.

[33] Drizyte-Miller K, Engstrom LD, Klomp JA, et al. Combination of the MTA-Cooperative PRMT5 Inhibitor BMS-986504 and KRAS Inhibitors Is an Effective Treatment Strategy for MTAP-Deleted KRAS-Mutant Pancreatic Cancer. [J]. Cancer Res, 2025,85,3540. http://dx.doi.org/10.1158/0008-5472.Can-25-1507.

[34] Rodon J, Prenen H, Sacher A, et al. First-in-human study of AMG 193, an MTA-cooperative PRMT5 inhibitor, in patients with MTAP-deleted solid tumors: results from phase I dose exploration. [J]. Ann Oncol, 2024,35,1138. http://dx.doi.org/10.1016/j.annonc.2024.08.2339.

[35] Zhang C and Zhuang S. The role of protein arginine methyltransferases in kidney diseases. [J]. Clin Sci (Lond), 2020,134,2037. http://dx.doi.org/10.1042/cs20200680.

[36] Che P, Yu L, Friedman GK, et al. Integrin αvβ3 Engagement Regulates Glucose Metabolism and Migration through Focal Adhesion Kinase (FAK) and Protein Arginine Methyltransferase 5 (PRMT5) in Glioblastoma Cells. [J]. Cancers (Basel), 2021,13,http://dx.doi.org/10.3390/cancers13051111.

[37] Huang L, Liu J, Zhang XO, et al. Inhibition of protein arginine methyltransferase 5 enhances hepatic mitochondrial biogenesis. [J]. J Biol Chem, 2018,293,10884. http://dx.doi.org/10.1074/jbc.RA118.002377.

[38] Şenbabaoğlu Y, Gejman RS, Winer AG, et al. Tumor immune microenvironment characterization in clear cell renal cell carcinoma identifies prognostic and immunotherapeutically relevant messenger RNA signatures. [J]. Genome Biol, 2016,17,231. http://dx.doi.org/10.1186/s13059-016-1092-z.

[39] Thompson RH, Dong H, Lohse CM, et al. PD-1 is expressed by tumor-infiltrating immune cells and is associated with poor outcome for patients with renal cell carcinoma. [J]. Clin Cancer Res, 2007,13,1757. http://dx.doi.org/10.1158/1078-0432.Ccr-06-2599.

[40] Rathmell WK, Rumble RB, Van Veldhuizen PJ, et al. Management of Metastatic Clear Cell Renal Cell Carcinoma: ASCO Guideline. [J]. J Clin Oncol, 2022,40,2957. http://dx.doi.org/10.1200/jco.22.00868.

[41] Stupichev D, Miheecheva N, Postovalova E, et al. AI-driven multimodal algorithm predicts immunotherapy and targeted therapy outcomes in clear cell renal cell carcinoma. [J]. Cell Rep Med, 2025,6,102299. http://dx.doi.org/10.1016/j.xcrm.2025.102299.

[42] Shah AY, Kotecha RR, Lemke EA, et al. Outcomes of patients with metastatic clear-cell renal cell carcinoma treated with second-line VEGFR-TKI after first-line immune checkpoint inhibitors. [J]. Eur J Cancer, 2019,114,67. http://dx.doi.org/10.1016/j.ejca.2019.04.003.

[43] Li M, Zhang Y, Jiang W, et al. ID1 boosts antiviral immunity by countering PRMT5-mediated STING methylation. [J]. Cell Rep, 2025,44,116547. http://dx.doi.org/10.1016/j.celrep.2025.116547.

[44] Zhang H, Shi G, Li Y, et al. Epigenetically targeting PRMT5 promotes antitumor immunity by inducing endogenous retroviruses expression and triggering viral mimicry response. [J]. Transl Res, 2025,281,55. http://dx.doi.org/10.1016/j.trsl.2025.05.007.

[45] Kim H, Kim H, Feng Y, et al. PRMT5 control of cGAS/STING and NLRC5 pathways defines melanoma response to antitumor immunity. [J]. Sci Transl Med, 2020,12,http://dx.doi.org/10.1126/scitranslmed.aaz5683.

[46] Zhang Q, Ding L, Yan Y, et al. Decoding sunitinib resistance in ccRCC: Metabolic-reprogramming-induced ABAT and GABAergic system shifts. [J]. iScience, 2024,27,110415. http://dx.doi.org/10.1016/j.isci.2024.110415.

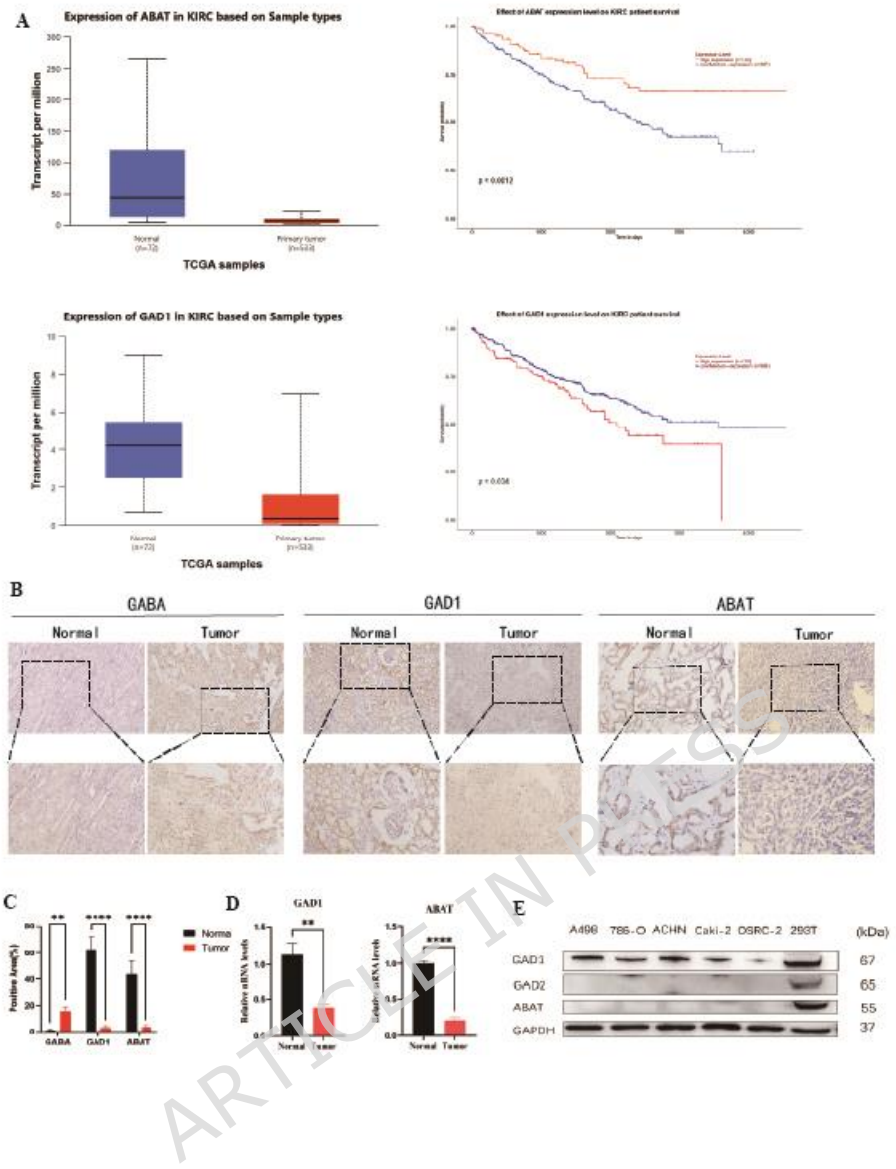

Figure 1.ABAT expression is significantly downregulated in renal cell carcinoma.(A) Expression levels of ABAT and GAD1 in ccRCC from The Cancer Genome Atlas (TCGA) database and their prognostic significance.(B) Representative immunohistochemical (IHC) staining of ABAT and GAD1 in clinical ccRCC tissue sections (n = 5).(C) Quantification of the proportion of IHC-positive cells.(D) RT-qPCR analysis of ABAT and GAD1 expression in ccRCC patient tissue samples (n = 5).(E) Western blot showing protein expression levels of ABAT, GAD1, and GAD2 in

renal carcinoma cell lines.Data are presented as mean ± SD. Statistical significance was determined by two-way ANOVA . *P < 0.05, **P < 0.01, ***P < 0.001.

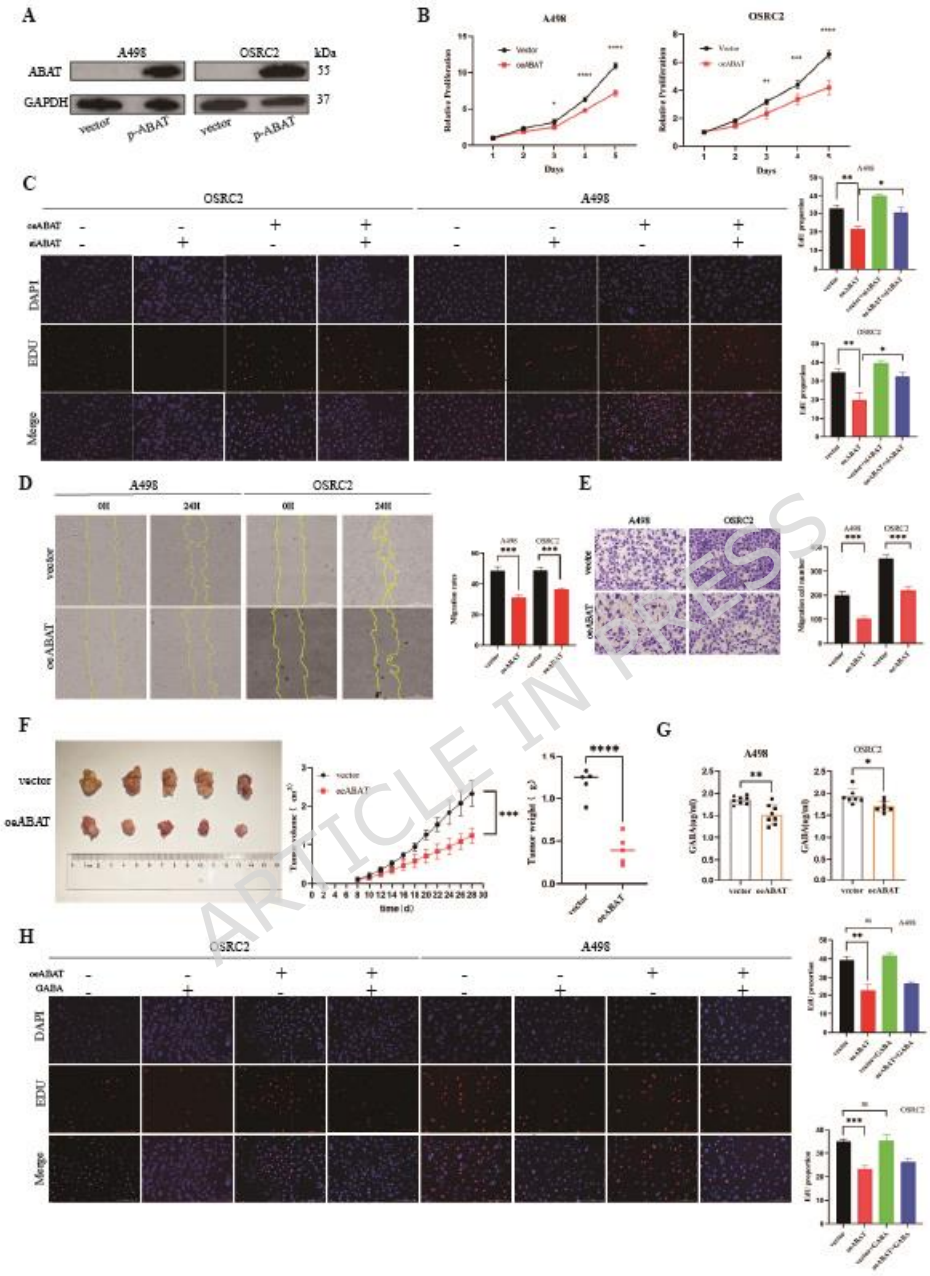

Figure 2.Overexpression of ABAT significantly suppressed tumor growth.(A) Western blot showing the overexpression level of ABAT in the indicated renal carcinoma cell lines.(B) CCK-8 assay demonstrating the proliferation of the indicated renal carcinoma cells, with daily measurements normalized.(C) EdU assay reflecting

the proliferation level of the indicated cells.(D) Wound healing assay showing that ABAT overexpression inhibited the migration of the indicated cells.(E) Transwell assay indicating that ABAT overexpression reduced the invasive ability of the indicated cells.(F) Xenograft tumor model illustrating tumor size and growth curves following ABAT overexpression.(G) GABA concentration in the supernatant of the indicated cells was measured using an ELISA kit.(H) The indicated cells were treated with 100 μM GABA or an equal volume of PBS for 12 h, followed by EdU assay.Data are presented as mean ± SD. Statistical significance was determined by two-way ANOVA. *$P < 0.05$, **$P < 0.01$, ***$P < 0.001$.

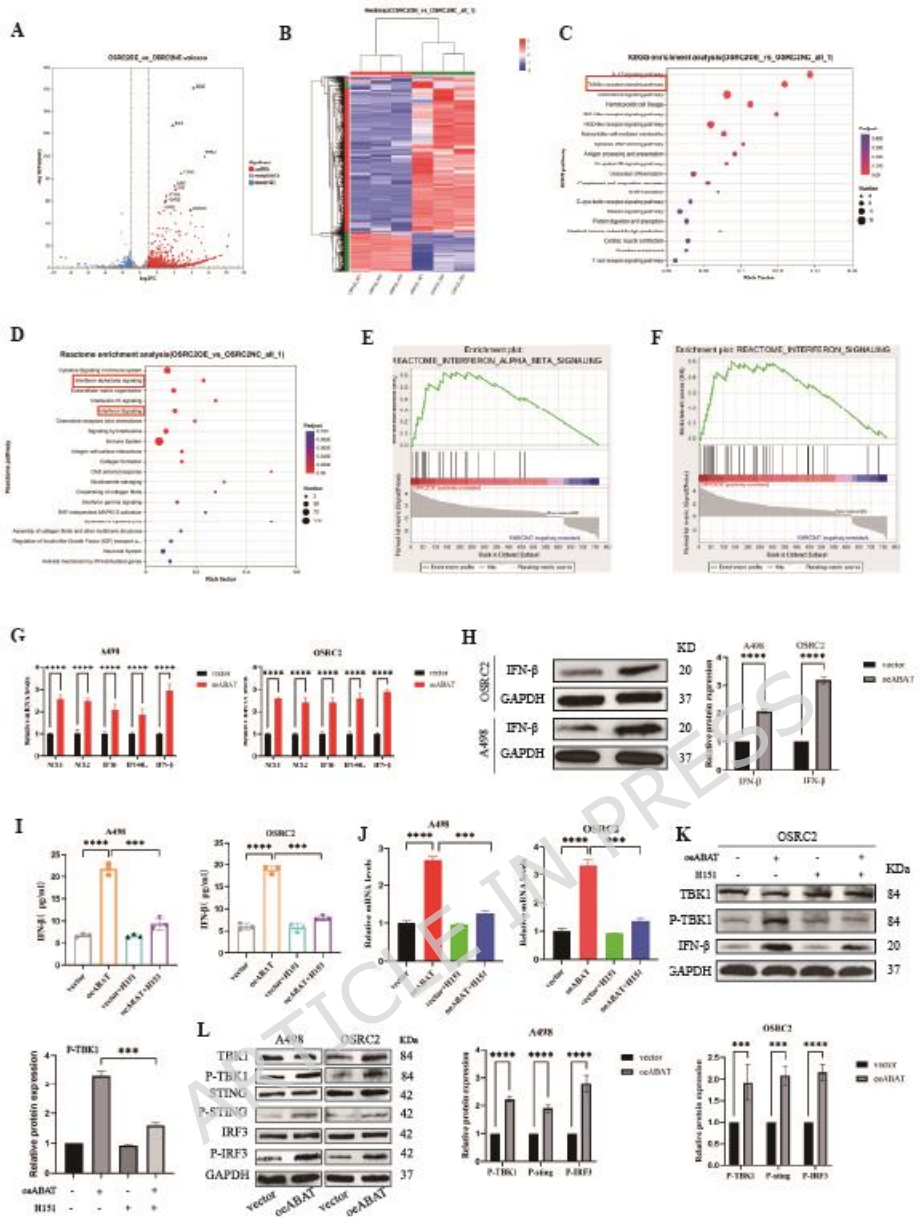

Figure 3.Overexpression of ABAT triggers cGAS-STING-induced type I interferon signaling.(A – B) Volcano plot and heatmap demonstrate differentially expressed mRNAs in the indicated OSRC2 cells.(C – D) Enrichment analysis of representative KEGG and Reactome pathways among oeABAT-mediated target genes.(E – F) GSEA plots of individual pathways enriched in shAsns-depleted MBT2 cells.(G) RT-qPCR shows mRNA levels of interferon-related genes in the indicated cells.(H) Western blot reveals IFN-β protein levels in oeABAT-expressing cells.(I –

K) ELISA, RT-qPCR, and Western blot indicate IFN-β levels in the indicated cells following H151 treatment.(L) Western blot displays protein levels of cGAS–STING pathway components in oeABAT-expressing cells.Data are presented as mean ± SD. Statistical significance was determined by two-way ANOVA. *P < 0.05, **P < 0.01, ***P < 0.001.

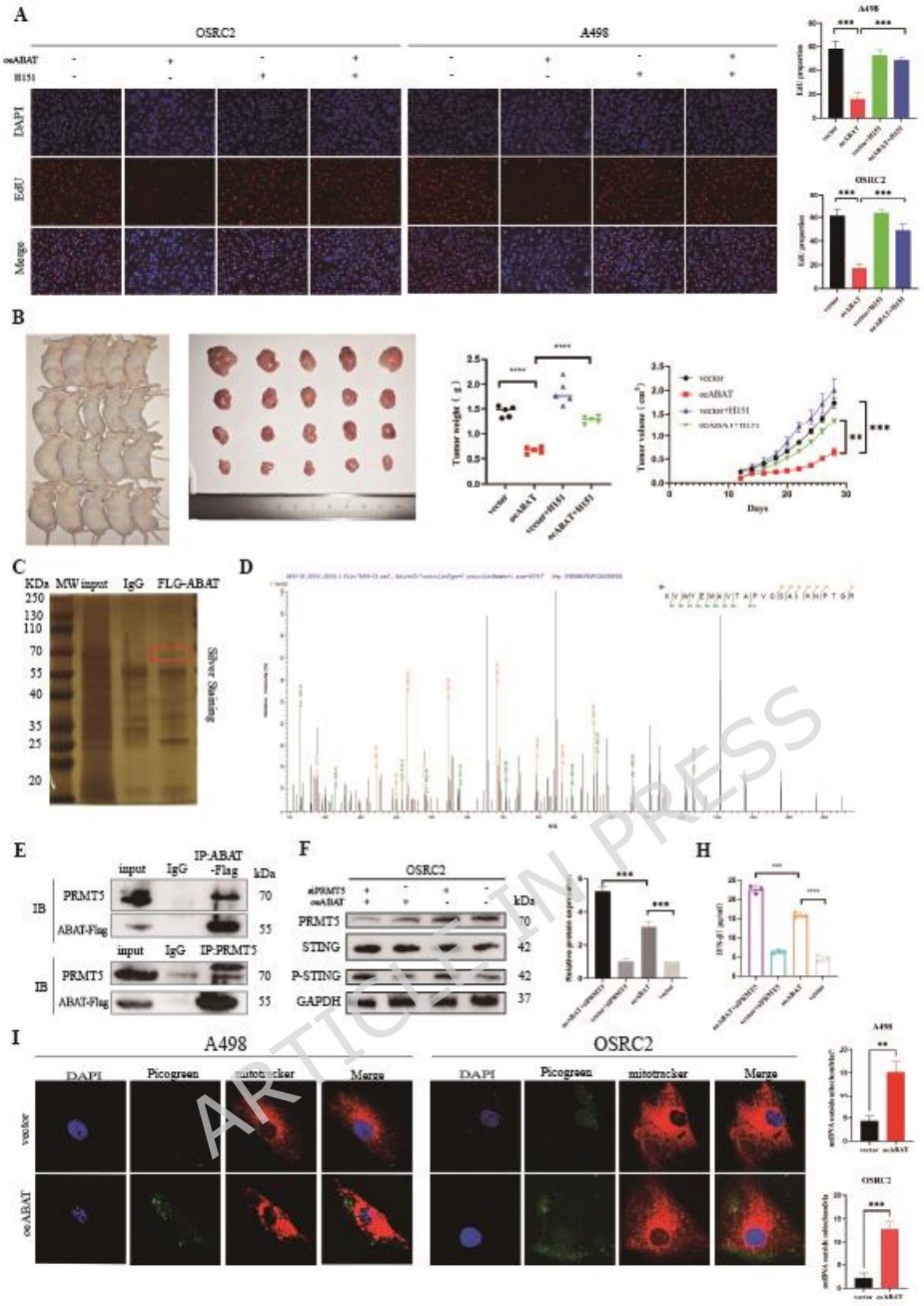

Figure 4.Overexpression of ABAT affects mitochondrial homeostasis and interacts with PRMT5.(A) EdU assay showing the proliferation of indicated cells following H151 treatment.(B) Xenograft tumor model (n = 5) demonstrating the in vivo tumorigenicity of indicated cells after H151 treatment.(C) Silver staining of the PAGE gel after co-immunoprecipitation in OSRC2 cells transfected with the FLAG-ABAT plasmid.(D) Secondary mass spectrometry (MS/MS) spectrum of a PRMT5-specific peptide.(E) Western blot indicating the interaction between ABAT

and PRMT5.(F-H) Western blot and ELISA showing the levels of STING and IFN-β after PRMT5 knockdown in control and oeABAT cells, respectively.(I) Quantification of the ratio of green fluorescence (DNA stained by Picogreen) co-localizing with mitochondria (stained by MitoTracker).Data are presented as mean ± SD. Statistical significance was determined by two-way ANOVA. *P < 0.05, **P < 0.01, ***P < 0.001.

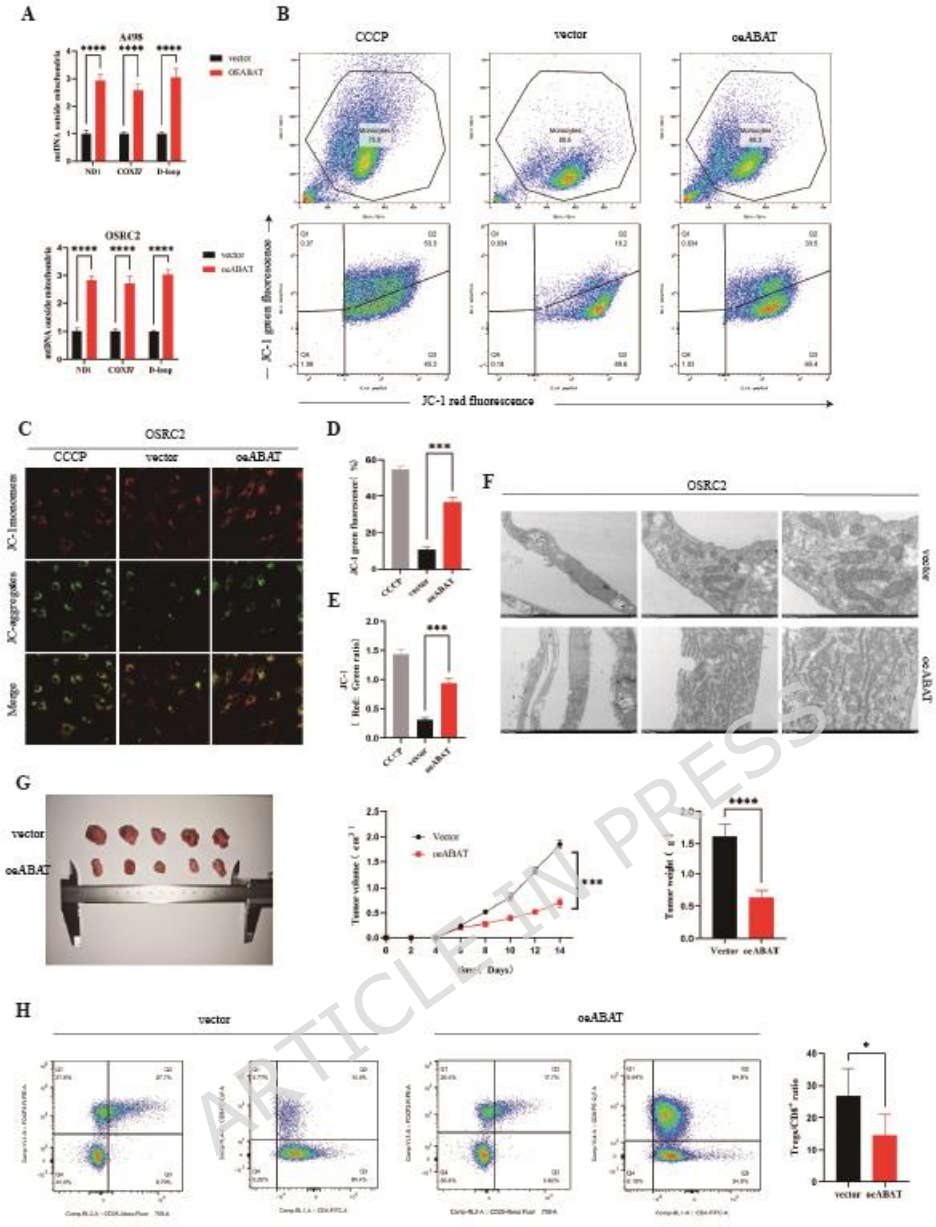

Figure 5.Overexpression of ABAT affects mitochondrial quality and reduces Treg cell infiltration in the tumor immune microenvironment.(A) RT-qPCR shows the relative levels of cytoplasmic mitochondrial DNA (cmtDNA) in the indicated cell lines.(B, D) Flow cytometry analysis displays the ratio of JC-1-positive cells and corresponding quantification in the indicated cells.(C, E) Representative confocal microscopy images of JC-1 staining in the indicated cells and the associated quantification.(F) Electron microscopy reveals the distinct morphological features of mitochondria.(G) Subcutaneous tumor formation assay (n = 5) demonstrates that

ABAT overexpression significantly suppresses tumor growth in vivo(H) Flow cytometric analysis of tumors from (G) showing the proportions of Tregs and $CD8^+$ T cells.Data are presented as mean ± SD. Statistical significance was determined by two-way ANOVA. *P < 0.05, **P < 0.01, ***P < 0.001.

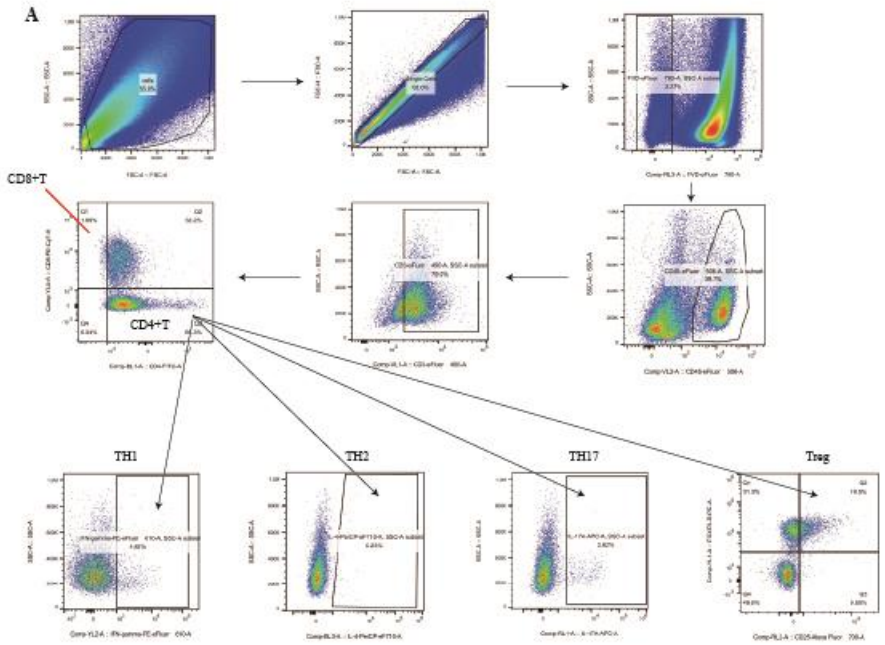

Figure S1.the gating strategy for murine tumor-infiltrating immune cells.（A）Representative flow-cytometry gating strategy for quantifying the number of various immune effector cell subsets in murine tumors.